Acta Materialia 168 (2019) 13–23

Contents lists available at ScienceDirect

Acta Materialia

journal homepage: www.elsevier.com/locate/actamat

Full length article

Particle deformation and microstructure evolution during cold spray of individual Al-Cu alloy powder particles

Tian Liu [a], Jeremy D. Leazer [b], Luke N. Brewer [a, *]

[a] University of Alabama, USA
[b] Naval Postgraduate School, USA

ARTICLE INFO

Article history:
Received 13 November 2018
Received in revised form
26 January 2019
Accepted 29 January 2019
Available online 1 February 2019

Keywords:
Cold spray deposition
Single particle impact
Al-Cu alloy
PED
TKD

ABSTRACT

This paper examines the single particle impact process for a series of Al-Cu alloy powder particles with 2–5 wt% copper, performed using a low-pressure cold spray system with helium as the carrier gas. The cold spray deposition process is fundamentally controlled by the deformation processes, which occur during single particle impacts. Single particle depositions on steel substrates were produced for each composition over a range of gas temperatures (225–325 °C). Cross sections from single, impacted particles were produced using focused ion beam methods. The deformation microstructure in individual cold sprayed particles was studied using precession electron diffraction (PED) and transmission Kikuchi diffraction (TKD) techniques. For Al-Cu alloy particles, the amount of deformation estimated using a compression ratio did not show a significant difference with varying copper alloy additions. The single particles experienced large deformation upon impact, and ultrafine grains were formed at the particle/substrate interface via dynamic recrystallization. The particles were bonded to the steel substrate via a thin amorphous layer at the interface.

1. Introduction

Cold gas-dynamic spray [1], or cold spray (CS), is becoming popular as a solid-state material deposition process which impacts fine, metallic particles at supersonic velocities onto a substrate. A coating produced using the cold spray process is built up by the impacts of many millions of particles. Two types of bonding are involved in this process: particle-onto-substrate, and particle-onto-particle [2]. As single particle impacts are the building blocks for cold sprayed materials, it is essential to understand the deformation processes that occur and the microstructures that form as each particle impacts the underlying substrate.

During CS, bonding occurs if an impacting particle reaches a sufficiently high velocity, the so-called critical velocity [3–5]. When an individual particle impacts onto a substrate, the particle will experience a large deformation at an extremely high strain rate in the range of 10^6-10^9/s [3,6–10], accompanied by heat generation. The contact time, which is the time from first contact to complete conversion of the particle kinetic energy to internal energy, is typically less than 100 ns [10]. Plastic strain is concentrated in the shear zones at the particle/substrate interface [10]. As strain localization and heat energy accumulate, an adiabatic shear instability (ASI) will develop at the interface. ASI is often used to describe the bonding mechanisms for cold spray deposition [6,9,11–15]. However, there is some recent debate on the role of ASI for particle bonding [16–18]. Hassani-Gangaraj et al. argue that the shock-induced pressure waves upon impact cause material jetting, and this process is the central mechanism for particle bonding [16]. More high spatial resolution experimental data will be essential for providing further clarity on the nature of the interface after particle impact and on the mechanism of bonding.

The impact-induced deformation behaviors, as characteristics of the CS process, can be inferred from the deformed microstructures of the deposited particles after spray. The literature on single particle impacts has often quantified the total particle deformation by measuring a flattening or compression ratio. These terms are used differently in the literature, and for this paper, we will follow the naming conventions of Li et al. [19,20]. In this work, the compression ratio will be described in detail in the experimental methods section; briefly, the compression ratio is the average strain or shape distortion along the deposition direction in a single, originally spherical, particle after impact. King et al. found that the local compression ratio (local average strain) of cold sprayed copper

* Corresponding author.
E-mail address: lnbrewer1@eng.ua.edu (L.N. Brewer).

https://doi.org/10.1016/j.actamat.2019.01.054
1359-6454/

particles increased from the top surface of the particle towards particle/substrate interface [21], and they reported that the compression ratio of Al, Cu [22], and Ti particles [13] increased initially with increasing particle size, and then approached some maximum ratio. Alkhimov et al. [23] studied the impact of aluminum particles onto different substrates, and found that the compression ratio was determined by $\rho_p v_p^2/H_p$, and was not influenced significantly by the ratios of ρ_p/ρ_s or H_p/H_s, where v_p is the impact velocity, and ρ_p, ρ_s, H_p, and H_s are the density and dynamic hardness values of the particle and substrate, respectively. Assadi et al. [4] found that the compression ratio was linearly related to the ratio of particle velocity to the critical velocity based on their simulation work. Overall, the compression ratio has been widely used to indicate how much a single particle is flattened upon impact during cold spray, as summarized in Table 1.

The compression ratio is helpful, but it is insufficient to provide a complete description of the particle deformation as it does not quantify or provide detail on the level or distribution of deformation in a particle interior. While spatially-resolved, crystallographic information is essential for understanding the deformation process, the levels of plastic strain and the small length scale for a single particle are beyond the spatial resolution of standard electron backscatter diffraction (EBSD) mapping techniques. Transmission Kikuchi diffraction (TKD) and precession electron diffraction (PED), newer, higher spatial resolution electron diffraction tools, are popular orientation microscopy techniques developed for and applied to nanocrystalline materials and nanostructures in recent years. TKD, introduced by Keller and Geiss [24], is an alternative approach to electron backscatter diffraction (EBSD) in the scanning electron microscope (SEM). Although TKD, also known as transmission EBSD (*t*-EBSD), is performed on the same instrument and with the same detector as conventional EBSD, the spatial resolution of TKD (down to several nanometers) is significantly improved by using a thin, electron transparent specimen [25]. PED, a transmission electron microscope (TEM)-based orientation microscopy technique developed by Vincent and Midgley [26], is very suitable for the characterization of ultrafine-grained microstructures as well [27]. These two techniques are both applied in this work to enable mapping of the crystallography of single deposited particles.

This work aims to study the single particle impact process of a series of Al-Cu binary alloy powders with 2–5 wt% copper onto a steel substrate. The Al-Cu binary alloy system was selected on account of its well-known attributes in the physical metallurgy literature and its technological importance as the parent alloys for Al-Cu alloys, e.g. AA2014, AA2024, AA 2099 and AA2219. This paper provides the first, detailed crystallographic information about single impacted particles, especially for the ultrafine grain structures located at the particle/substrate interface. It will be illustrated how single Al-Cu alloy particles deform and adhere to the substrate during the impact process. Further, the influence of systematic copper alloy additions on the deformation behavior and microstructure evolution of the Al-Cu particles during the impact process will be described.

It is important to briefly review the starting microstructure of the feedstock material before studying the single impact process. The feedstock, inert gas atomized, Al-Cu powders displayed a cellular solidification microstructure with relatively low intragranular misorientation, as shown in Fig. 1. Previous work by Liu et al. [28], showed that the average grain sizes of Al-2 wt% Cu and Al-5 wt% Cu powders were 2.7 μm and 2.4 μm, respectively, while the average cellular spacings of Al-2 wt% Cu and Al-5Cu wt% powders were 1.9 μm and 1.6 μm, respectively. The as-atomized Al-Cu alloy powders consisted of α-Al as the matrix phase with a network of θ (Al_2Cu) phase segregated along the cell boundaries (brighter phase in Fig. 1 (a, b)). The θ phase fraction in the as-atomized powders systematically increased from 0.4 to 4.9 wt% with copper alloy additions [28].

2. Experimental methods

A modified cold spray deposition experiment was performed for Al with 2–5 wt% Cu alloy powder particles onto high strength steel 4340 substrates using a Centerline SST Model Series C low-pressure cold spray system under different spray conditions, as described in Table 2. Steel 4340 substrates were purchased from Full Spectrum Machining in Gilroy, California for this experiment. The substrates were 50 mm by 100 mm rectangular plates that were 6.35 mm in thickness. These plates were diamond polished to a 1 μm finish. The powder feed rate during deposition was lowered until single particles impacted and adhered to the substrate. Throughout this paper, the alloy particles will be referenced, based on their nominal compositions, as Al-XCu, e.g. Al-2 wt% Cu is Al-2Cu. The feedstock Al-Cu powders were produced via inert gas atomization process using nitrogen gas by Valimet, Inc. from Stockton California [28]. The Al-Cu powders were sized for CS to a particle diameter ranging from 10 μm to 45 μm with a median size between 22 and 26 μm.

The total particle deformation after impact can be described by the compression ratio, R_c. The compression ratio is expressed as the following equation [19,20]:

$$R_c = \frac{d_0 - h}{d_0} \quad (1)$$

where d_0 is diameter of a spherical particle before deformation and h is the height of the deformed particle. A compression ratio approaching 1 would indicate a completely flattened particle, while a compression ratio approaching 0 would describe a spherical particle. The deformed particles were dissected to measure these dimensions using a FEI Quanta 3D Dual Beam instrument. Approximately 10 deposited particles with an estimated original particle diameter [22] of approximately 14–30 μm were dissected for each alloy sprayed at 325 °C and additional two conditions for

Table 1
Compression ratios of impacted particles in the cold spray process.

Reference	Compression Ratio	Additional Information	Material
King et al. [21]	0.15	close to particle top surface	Cu onto Cu
	0.5	near particle/substrate interface	
King et al. [22]	0.17–0.6 for Al	particle diameter 2–25 μm	Al onto PZT
	0.35–0.7 for Cu	particle diameter 1–8 μm	Cu onto alumina
King et al. [13]	0.25–0.3	particle diameter 6–30 μm	Ti onto Ti
Alkhimov et al. [23]	0.35–0.47	particle diameter 10–30 μm	Al onto Cu
	0.37–0.63		Al onto unhardened steel
	0.44–0.72		Al onto hardened steel
Assadi et al. [4]	0.2–0.7 for Cu	simulated compression ratios increase with increasing particle velocity	Cu or Al particles onto a rigid substrate
	0.2–0.8 for Al		

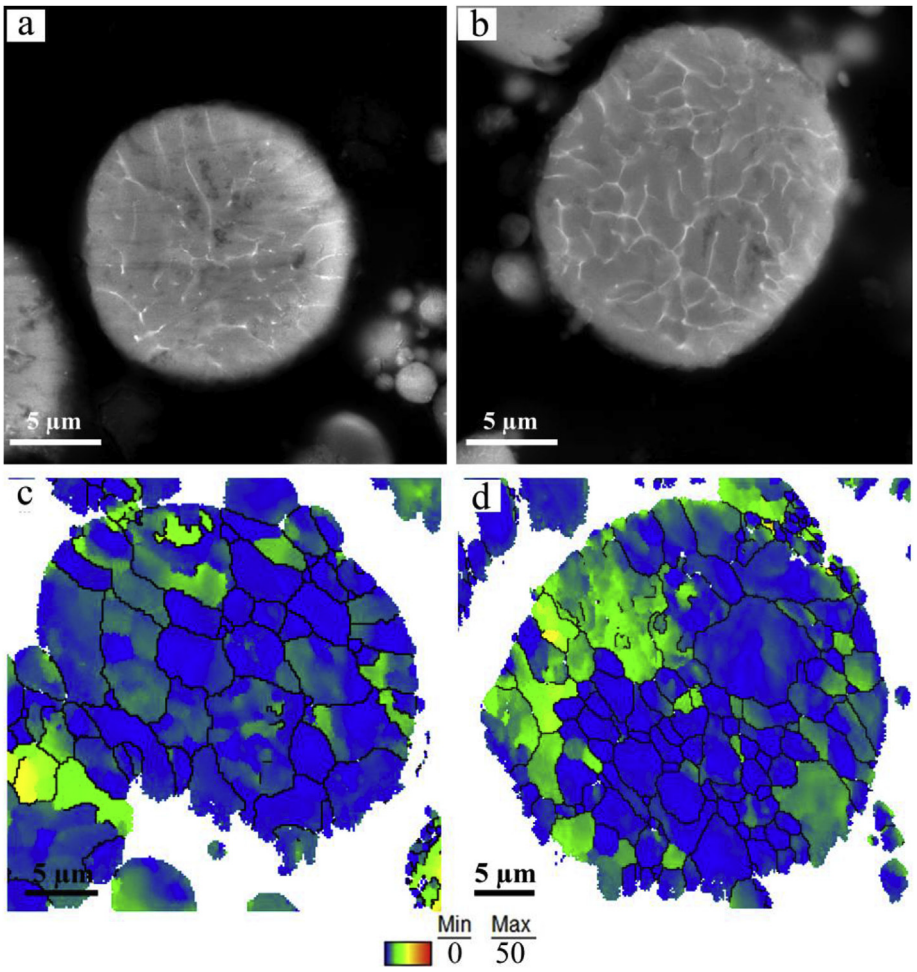

Fig. 1. Microstructure of feedstock Al-2wt% Cu (left column) and Al-5 wt% Cu (right column) powders, (a, b) backscatter electron images (θ phase is brighter), (c, d) intragranular misorientation as shown by grain reference orientation deviation (GROD) maps, the legend of GROD maps is shown in the bottom, high-angle grain boundaries (>10°) in black were overlaid in (c) and (d).

Table 2
Experimental conditions for single particle impact.

Powder (Al-Cu with varying amounts of Cu)	2 wt%, 3 wt%, 4 wt%, 5 wt%
Gas	He
Substrate Material	4340 steel
Nozzle	PBI epoxy (2 mm throat diameter, 120 mm divergent barrel, 6.3 mm exit diameter)
Gas Temperature (°C)	225, 275, 325
Gas Pressure (MPa)	1.21

Al-2Cu alloy (sprayed at 225 °C and 275 °C) using a gallium ion beam at 30 keV. The height of the deformed particle was obtained from the expression [22]:

$$h = h_m/\sin\alpha \quad (2)$$

where h_m is the measured particle height, α is the stage tilt angle. Further, d_0 was calculated using an ellipsoidal model proposed by King et al. [22]:

$$d_0 = \sqrt[3]{w^2 h} \quad (3)$$

where w is the width of the deformed particle.

Ten cross sections of the deposited Al-2Cu and Al-5Cu particles containing the interfacial region between particle and substrate were lifted out using a FEI Quanta 3D Dual Beam instrument. The selected deposited particles were approximately 15 μm in width. Then the specimens were thinned to electron transparency using a gallium ion beam at 30 keV, and finally polished at 5 keV using Tescan Lyra FIB-FESEM. The thin foils were characterized using a FEI Tecnai F-20 Scanning/Transmission Electron Microscope ((S)TEM) operated at 200 keV, equipped with a CCD camera, a high angle annular dark field (HAADF) detector, and EDAX energy dispersive X-ray system. Precession electron diffraction (PED), a TEM-based technique, was performed on the thin foils via a NanoMegas ASTAR platform [29] using a precession angle of 0.3° and a step size of 20–25 nm. Two of the TEM foils were analyzed in the JEOL 7000 FE Scanning Electron Microscope and Oxford Aztec EBSD system using transmission Kikuchi diffraction (TKD) technique. The foils were tilted 20° away from the EBSD detector and the working distance was set at approximately 3 mm. The TKD data was acquired using an accelerating voltage of 30 keV and a step size of 25 nm. The PED and TKD data processing was performed using EDAX-TSL OIM Analysis 7 software. The grain dilation cleanup method was applied on the PED and TKD data using a grain tolerance angle of 10° and a minimum grain size of 5 pixels. In this process, < 3% of TKD data was modified and <6% of PED data was

modified. In addition, a 180° ambiguity correction was used for the PED data prior to grain dilation. The kernel average misorientation (KAM) and grain reference orientation deviation (GROD) maps were generated to reveal the level of plastic deformation in the deformed particles. The GROD map displays the deviation in orientation of a point within a grain from the reference orientation for the grain to which the point belongs. The reference orientation for each individual grain in this work was chosen as the orientation of a point in the grain with the lowest kernel average misorientation [30–32]. The KAM map presents the average misorientation between each data point and its nearest neighbors excluding misorientations greater than 5° [30] for this work. It should be noted that three Al-2Cu and three Al-5Cu particles sprayed at 325 °C were prepared for grain size measurements, and 187 grains of Al-2Cu and 353 grains of Al-5Cu in total were measured, respectively.

3. Results

3.1. Morphologies of deposited particles and amount of particle deformation

During cold spray, the Al-Cu alloy particles were heavily deformed. Morphologies of the Al-Cu alloy particles after impact onto the steel substrate are shown in Fig. 2 and Fig. 3. From the top-down view of deposited Al-Cu particles (Fig. 2), jet-like features were observed in the peripheral region of particles. It should be noted that the jetting features were not continuous around the particle, but instead showed multiple small fractures around the periphery of the impacted particle. No clear, qualitative difference in top-down impact morphology for different Al-Cu compositions was observed. Smaller particles were deposited on the top of some of the particles (e.g. Fig. 2 (d)). Fig. 2 (a) showed a crater from a small particle that impacted the particle under observation but did not adhere. The steel substrate was much harder than the impacting aluminum alloy particle, and as such, almost no penetration of the particle into the substrate was noted for any of the

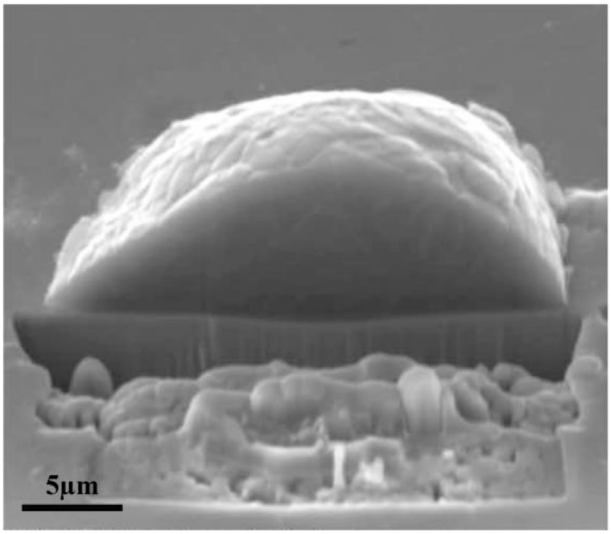

Fig. 3. Secondary electron image (stage tilt 52°) of a dissected Al-4Cu alloy particle sprayed at 325 °C.

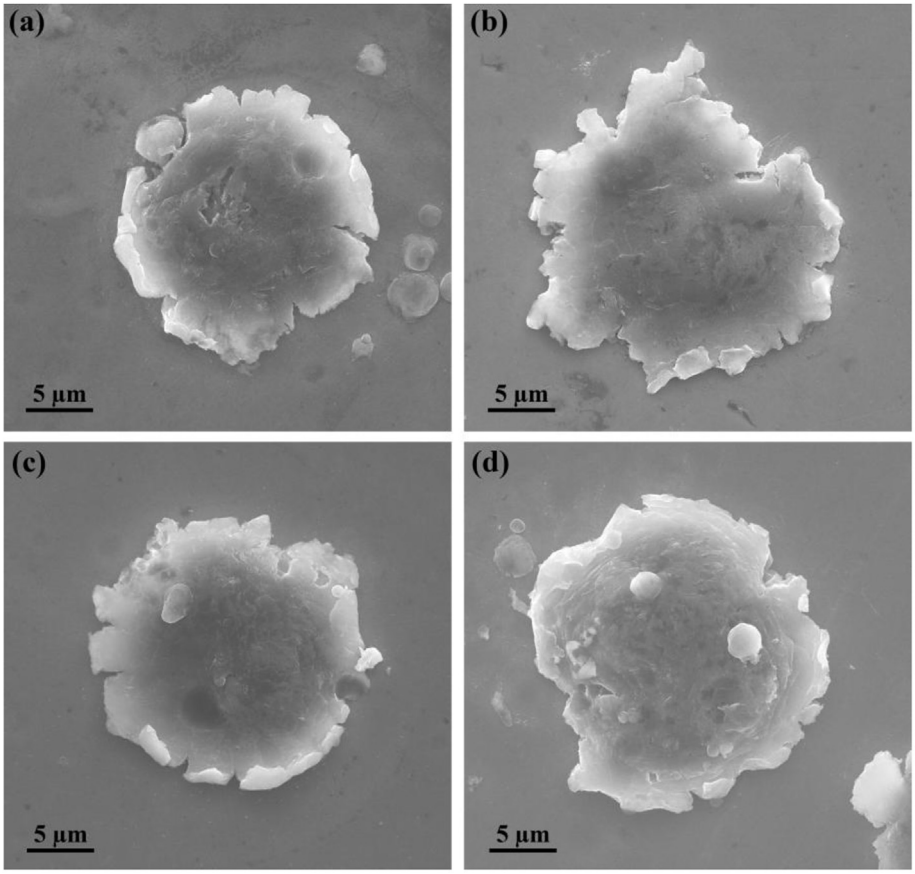

Fig. 2. Secondary electron images of individual deposited particles (top-down view), (a) Al-2Cu, (b) Al-3Cu, (c) Al-4Cu, and (d) Al-5Cu sprayed at 325 °C.

compositions (Fig. 3).

In general, the degree of particle deformation, as quantified by the compression ratio, did not vary significantly with increasing copper content or increasing gas temperature (Fig. 4 and Fig. 5). The average compression ratio from Al-2Cu to Al-5Cu was 0.59 ± 0.06, 0.57 ± 0.11, 0.52 ± 0.06, and 0.55 ± 0.06, respectively (Fig. 4). Generally, the average compression ratio slightly decreased with copper alloy additions from 2–3 wt% Cu to 4–5 wt% Cu. The change in compression ratio with increasing gas temperature was also slight in the given temperature range from 225 °C to 325 °C. The Al-2Cu alloy sprayed at 225 °C exhibited the lowest average compression ratio of 0.56 ± 0.06, while the average compression ratio for the Al-2Cu alloy sprayed at 275 °C and 325 °C was 0.62 ± 0.04 and 0.59 ± 0.06, respectively (Fig. 5).

3.2. Deformation microstructure in single deposited particles

The deposited particles were severely deformed, but the deformation was not uniformly distributed. Fig. 6 (a, b) and Fig. 7 (a, b) display the morphology and microstructure of the deformed particles' cross sections, and the impact direction is vertical in these images. The θ phase network was still observed in the particles after impact (bright phases Figs. 6 and 7 (b)), as was the case in the feedstock powders (Fig. 1). Generally, the α-Al cells became increasingly deformed from the top surface of the particle towards the particle/substrate interface, e.g. the aspect ratio of the Al-5Cu cells increased from 1.3 to 6.2 from the top surface towards the interface according to Fig. 7 (b). This increasing level of plastic deformation towards the interface was further confirmed by the KAM map (Figs. 6 and 7 (f)), in which the blue color suggests low deformation, and green to yellow colors indicate relatively higher deformation. Elongated cells observed near the particle/substrate interface were probably formed during the shearing process of the particle leading edge upon impact. Furthermore, substantial grain refinement occurred at the particle/substrate interfaces (Fig. 6 (c, d) and Fig. 7 (c, d)). The ultrafine grains at the interfacial region were very likely formed via dynamic recrystallization [33–36], as indicated by the low intragranular misorientation (blue grains) in the GROD maps (Figs. 6 and 7 (e)). The level of intragranular misorientation, as presented in the GROD maps, has clearly increased upon impact when compared with the same maps for the feedstock particles (see Fig. 1).

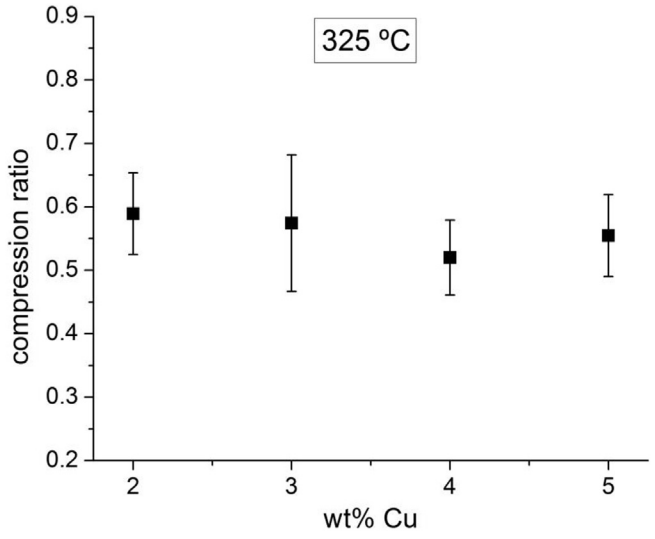

Fig. 4. Compression ratio as a function of Cu contents of Al-Cu alloys sprayed at 325 °C.

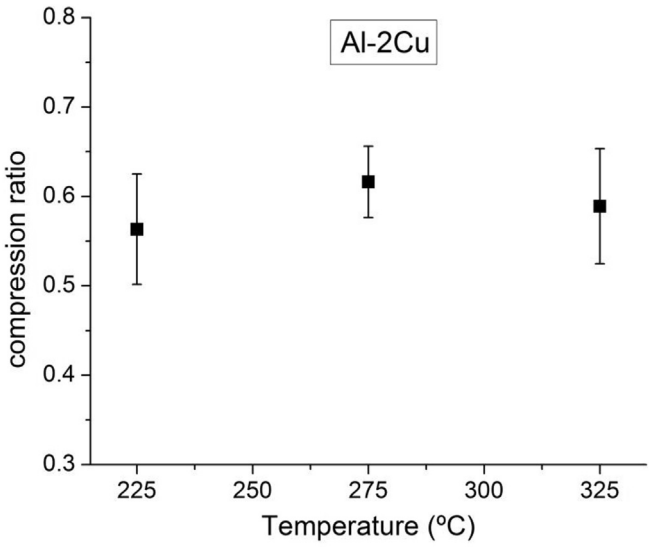

Fig. 5. Compression ratio as a function of gas temperature for the Al-2Cu alloy.

The manner in which different misorientation mapping schemes display deformation are clearly visible in Figs. 6 and 7 and can be used to assess different aspects of the deformation distribution in the impacted particles. KAM maps are based upon a very local quantification of misorientation, i.e. between an individual pixel and its nearest neighbors [30]. As such, this mapping technique is effective at showing the disritbutions of very local deformation in the microstructure. In the case of Figs. 6 and 7 (f), the density of deformation is clearly shown by KAM maps to be less at the top of the particle, to increase towards the particle/substrate interface, and then to decrease again for the small grains right at the interface. However, these small grains are difficult to observe in these KAM maps. For GROD maps (Figs. 6 and 7 (e)), these small interface grains are clearly visible by their uniform blue color. GROD maps are generated from the KAM maps by selecting a reference orientation as the pixel with the lowest KAM value for each individual grain. Any pixel of a grain colored blue in a GROD map is very close to the reference orientation of the grain, while any pixel colored yellow or red shows larger deviation from the reference orientation. Uniformly blue grains in a GROD map indicate recrystallized grains. A grain containing a color gradient from blue to yellow to red colors in a GROD map indicates higher levels of intragranular misorientation within one grain, and thus correlates with larger degrees of plastic deformation. The upper left section of the particle in Fig. 6 (e) appears in the GROD maps as being heavily deformed. The reason for the red coloration at the top of the particle is due to the reference pixel for that grain being much closer to the interface. The red region is simply highly misorientated from that reference pixel. The corresponding KAM map, Fig. 6 (f), more clearly presents that less deformation is present at the top left of this particle, and the deformation is instead concentrated towards the particle/substrate interface.

A similar grain size distribution (Fig. 8) was observed in the deposited Al-2Cu and Al-5Cu particles based on the PED data, with number frequency peaked at a grain diameter of approximately 100 nm, and the number frequency peak of Al-5Cu is slightly higher than Al-2Cu. The average grain size of the deposited Al-2Cu and Al-5Cu particles was 256 nm and 216 nm, respectively. Despite this small *average* size, the orientation maps in Figs. 6 and 7 showed that the upper portions of the particle have grain sizes much larger than 1 μm. In comparison, the original, average grain size of the Al-

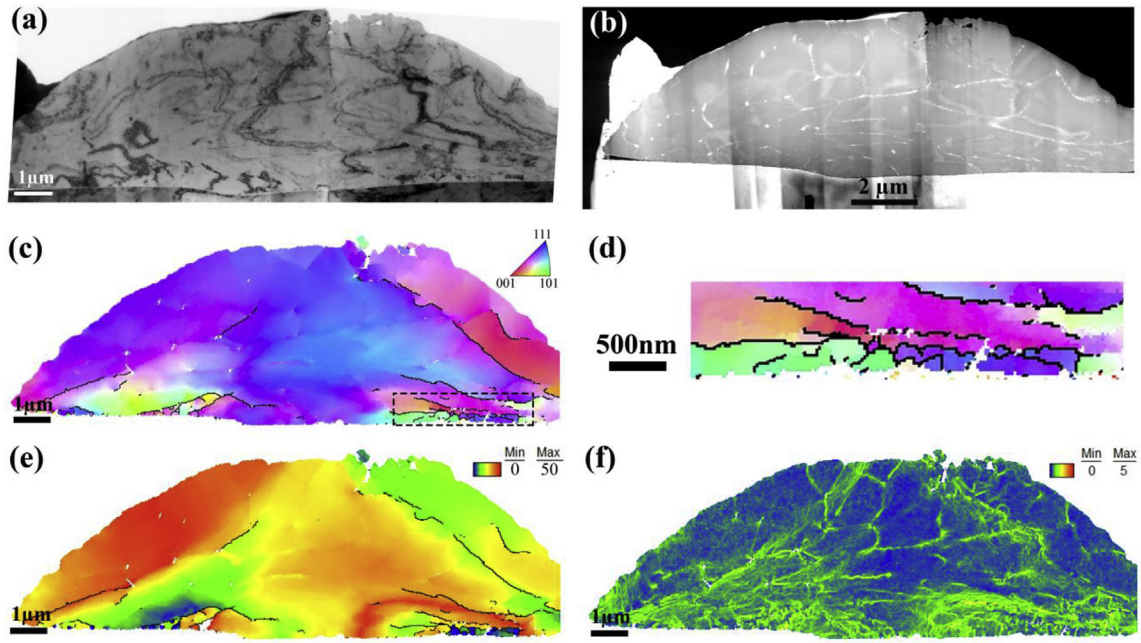

Fig. 6. Cross sections of a deposited Al-2Cu particle sprayed at 325 °C, (a) bright field TEM image, (b) STEM-HAADF image, TKD-based maps for the Al phase (c) orientation map with respect to z direction (out of the page), (d) a close-up view of the dashed rectangle region in (c), (e) GROD map, high-angle grain boundaries (>10°) in black were overlaid in (c–e), (f) KAM map.

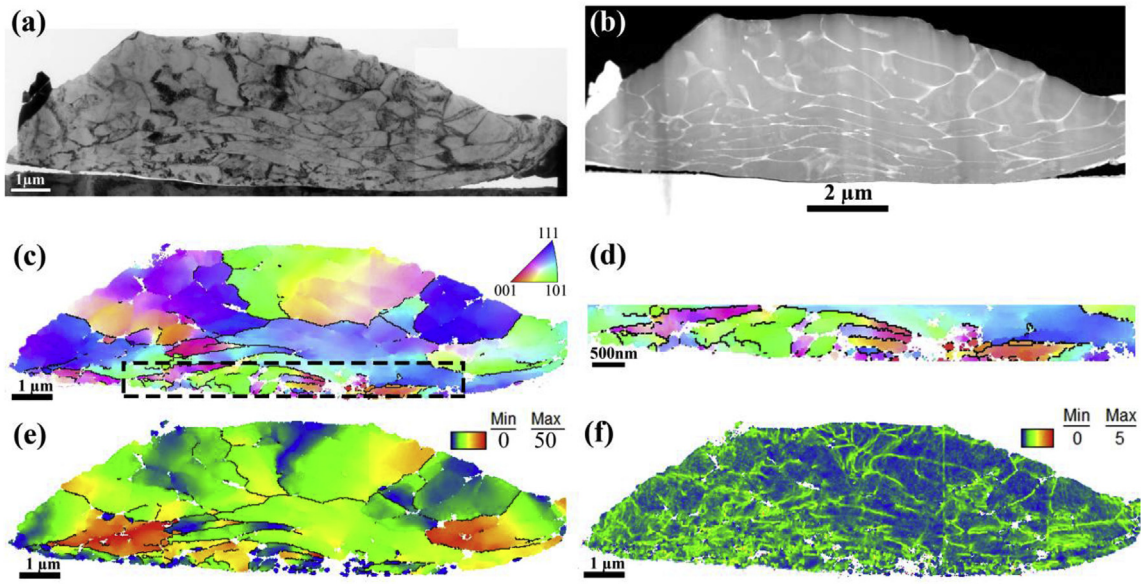

Fig. 7. Cross sections of a deposited Al-5Cu particle sprayed at 325 °C, (a) bright field TEM image, (b) STEM-HAADF image, TKD-based maps for the Al phase (c) orientation map with respect to z direction (out of the page), (d) a close-up view of the dashed rectangle region in (c), (e) GROD map, high-angle grain boundaries (>10°) in black were overlaid in (c–e), (f) KAM map.

2Cu and Al-5Cu feedstock powders was much larger, in the range of 2–3 μm in diameter [28]. More equiaxed, micron sized, grains were observed in the feedstock powder particles, while more flattened, or ultrafine (<500 nm diameter), grains were observed in the deposited particles.

In one particle cross section, we were able to observe the chance impact between exactly two particles (Fig. 9). The interface between these two Al-2Cu particles was very intimate. It was very difficult to discern the particle/particle boundaries compared with the particle/substrate boundaries from the TEM bright field (Fig. 9 (a)) or HAADF (Fig. 9 (b)) images. By performing the PED on this sample, the particle/particle boundary, as indicated by the red arrows in Fig. 9 (d), was clearly revealed by the elongated grains as well as the ultrafine grains with low intragranular misorientations (in blue color) at the interface. It was interesting to note that the width of this layer at the Al/Al interface was about 200–500 nm (Fig. 9(c–e)).

3.3. Bonding of individual Al-Cu particles onto steel substrate

The Al-Cu alloy particles were well bonded to the steel substrate. A very thin amorphous layer of approximately 10–15 nm in

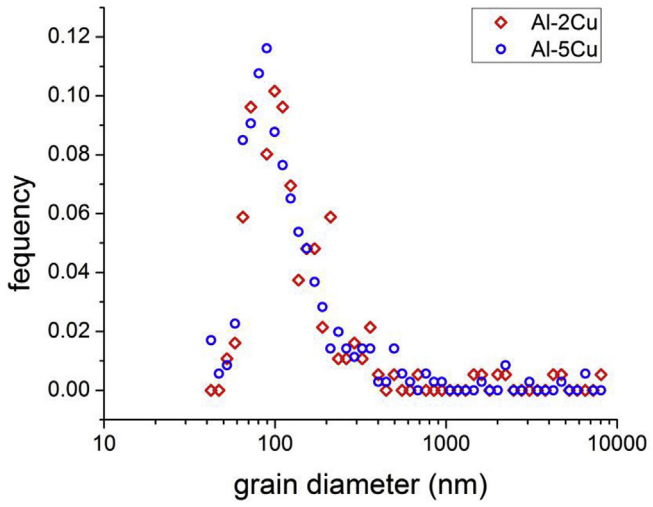

Fig. 8. Grain size distribution of individually deposited Al-2Cu and Al-5Cu particles sprayed at 325 °C (PED data).

thickness was observed in the interfacial region between the particle and substrate. This kind of amorphous layer was observed in several deposited particles, and one example is shown in Fig. 10. The exact elemental composition of this amorphous layer was unclear. The aluminum X-ray signal from the interface (black solid line in Fig. 10 (b)) was much suppressed in intensity compared with the aluminum matrix nearby (red dashed line in Fig. 10 (b)). The gallium signal from the aluminum matrix was due to the use of gallium ion beam during the TEM sample preparation. The relative intensity ratios of oxygen and carbon to aluminum in the interface were quite large, suggesting that this amorphous region was relatively rich in carbon and oxygen. However, it should be noted that the relative intensities for carbon and oxygen were similar between the interface region and the nearby aluminum. Only a minimal iron signal (small peak at 0.7 keV) was observed at the interface, indicating that the interface was not rich in iron. It should be noted that the Fe Kα peak intensity at 6.4 keV obtained from this interfacial region was also very small, and has been cropped for clarity in Fig. 10 (b). Future work using electron energy loss spectroscopy (EELS) should shed more light onto the composition of these amorphous interface layers.

4. Discussion

The measured compression ratios for these binary Al-Cu alloy particles were similar to previous work on cold spray of aluminum and were not sensitive to the copper content. We obtained an average compression ratio of 0.52–0.59 for Al-Cu particles (14–30 in diameter), while King et al. [22] found the compression ratio of aluminum particles (5–25 μm in diameter) sprayed onto PZT to be

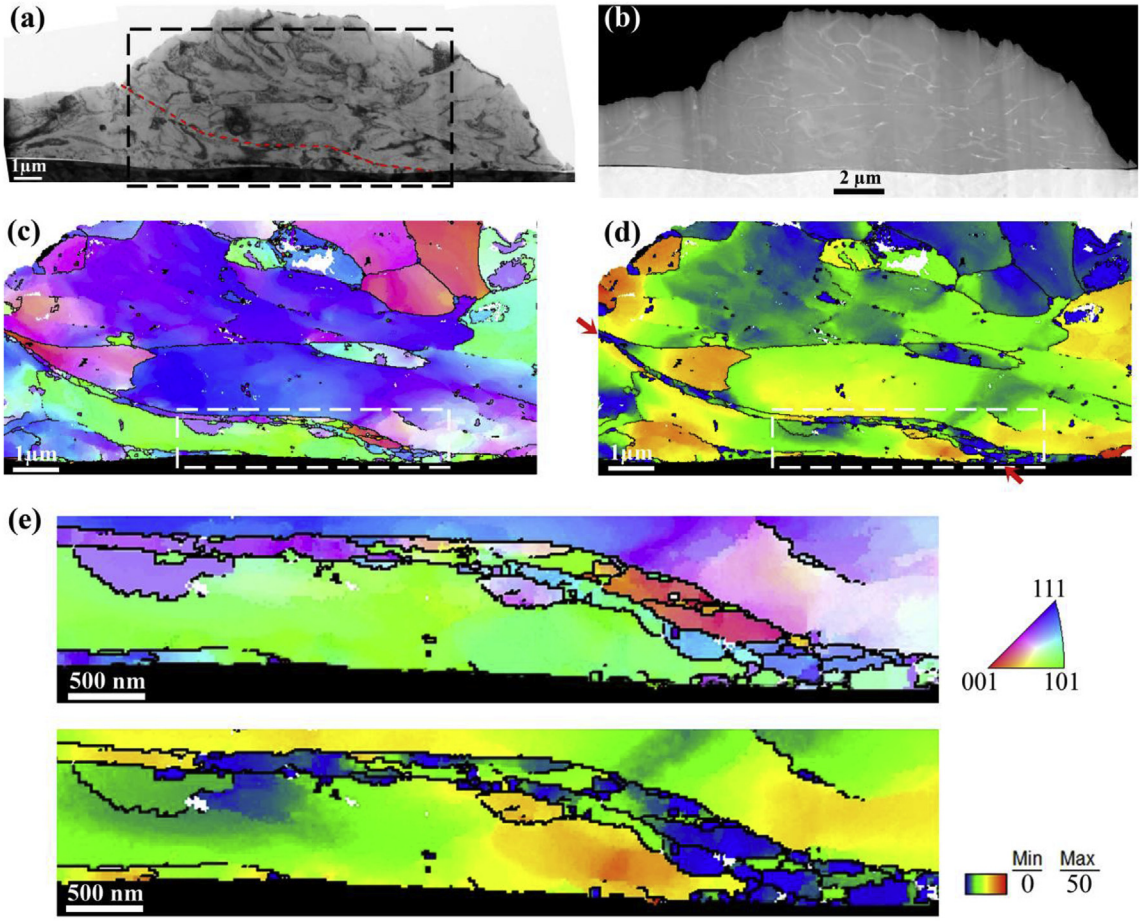

Fig. 9. Cross sections of two deposited Al-2Cu particles sprayed at 225 °C, (a) bright field TEM image, PED was performed on the black rectangle region, the red dashed line outlined the particle/particle interface, (b) STEM-HAADF image, PED-based maps for the Al phase (c) orientation map with respect to z direction (out of the page), (d) GROD map, the red arrows indicated the interface between deposited particles, (e) a close view of the white rectangle region in (c, d), high-angle grain boundaries (>10°) in black were overlaid in (c–e). (For interpretation of the references to color in this figure legend, the reader is referred to the Web version of this article.)

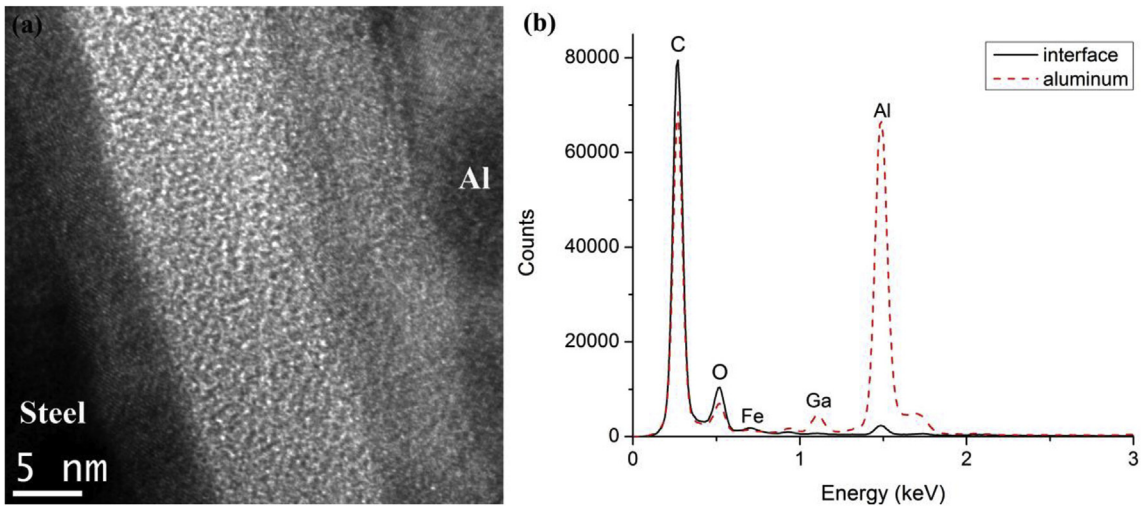

Fig. 10. High resolution TEM image of (a) an interfacial region between substrate and Al-2Cu particle sprayed at 325 °C, (b) EDX point spectra from the interface and adjacent aluminum matrix of the Al-2Cu particle shown in (a).

0.4–0.6. Assadi et al. [4] and Wong et al. [37] proposed that the compression ratio was a unique function of the ratio of particle velocity (v_p) to critical velocity (v_{cr}). In our laboratory, the particle velocity distributions for Al-2Cu and Al-5Cu alloys were measured via laser particle velocimetry and the deposition efficiency was also measured, when spraying the powders to produce thick deposits using helium gas at 325 °C/1.21 MPa. The critical velocity was obtained by comparing the particle velocity distribution and the corresponding deposition efficiency [38]. We obtained an average particle velocity of 618 m/s and an estimated critical velocity of 700 m/s for Al-2Cu particles, and an average particle velocity of 604 m/s and an estimated critical velocity of 730 m/s for Al-5Cu particles [39]. If the average particle velocity was used for a rough estimation of v_p/v_{cr}, the ratio of v_p/v_{cr} for Al-2Cu and Al-5Cu particles sprayed at 325 °C was approximately 0.88, and 0.83, respectively. Thus, the compression ratio of Al-2Cu would be expected to be similar to or slightly higher than Al-5Cu. In addition, the nanohardness of the Al-Cu feedstock particles was 1.24 ± 0.33 GPa, 1.28 ± 0.18 GPa, 1.32 ± 0.20 GPa, 1.52 ± 0.22 GPa with increasing copper contents from the recent work of Liu et al. [28]. The critical velocity would be expected to increase with the hardness of the particles [3,18]. As Al-5Cu is harder than Al-2Cu, theoretically, one would also expect that the compression ratio would slightly decrease from Al-2Cu to Al-5Cu. Such slight decrease in compression ratio can be captured from Fig. 4, but further discernment of differences is difficult due to the somewhat large error bars. We believe that more apparent differences in compression ratio might be observed, for powder particles with large differences in hardness.

We compare the compression ratios for cold sprayed pure aluminum and pure copper particles from additional low-pressure cold spray experiments. Single pure aluminum and pure copper particles were sprayed onto the steel substrates with nitrogen as the carrier gas. It should be noted that nitrogen gas produces lower particle velocities than helium [40]. The impact-induced deformation behavior of single particles depends on the hardness of the particle material and the substrate material [8]. The nanohardness of pure Al particles, pure Cu particles, and 4340 steel (quenched and tempered) was about 1.0 ± 0.1 GPa [41], 1.8 ± 0.2 GPa [42], and 5.3 ± 0.25 GPa [43], respectively. The aluminum particles (softest particle material) were highly flattened along the impact direction with no penetration into the substrate, whereas the copper particles (hardest particle material) showed much less deformation and penetrated into the substrate to about 0.8 μm in depth (Fig. 11). The average compression ratios for pure aluminum and pure copper were approximately 0.9 and 0.5, respectively. Adding copper as an alloying element to aluminum, the average compression ratio decreased from 0.9 (pure aluminum, softest) to a value of approximately 0.52–0.59 (Al-Cu particles with intermediate hardness), however, for Al-Cu binary alloy particles, the exact copper content did not exhibit a significant effect on the compression ratio (Fig. 4). In addition, the impacted Al-Cu particles did not show appreciable

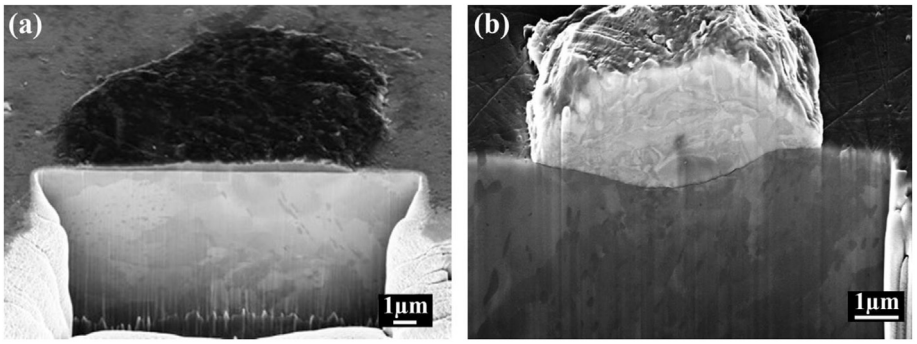

Fig. 11. Secondary electron images (stage tilt 54°) of dissected particles (a) pure Al sprayed at 150 °C, (b) pure copper sprayed at 300 °C, using nitrogen as the carrier gas.

penetration into the steel substrate. The steel substrate showed the least deformation as it is much harder than all the particle materials in these experiments.

In this work, the severity of deformation generally increased from the top surface of the particle towards the interface between particle and substrate. The cellular structure of the feedstock Al-Cu alloy powders was preserved in the deposited particles, albeit in a deformed version, and the cells became increasingly deformed towards the particle/substrate interface. King et al. [21] studied single particle impact of copper onto C11000 copper alloys, and also observed a tendency for the grains to become increasingly deformed from the top-center of the impacted particle towards the particle/substrate interface in any direction based on the inspection of ion beam images of the cold sprayed copper particle cross section. In this work, we successfully utilized electron diffraction tools (PED, TKD) to better quantify the level of plastic deformation inside a deposited particle. The KAM maps in Figs. 6 and 7, showed a non-uniform distribution of plastic deformation in the deformed particle interior. Larger intragranular misorientations (green to yellow color) were observed near the interfacial region, while smaller intragranular misorientations (blue) were shown towards the particle top surface, which indicated plastic deformation was more concentrated towards the interface.

A direct comparison between a single impacted Al-5Cu particle and an Al-5Cu coating after cold spray shows the importance of *subsequent* particle impacts after the initial impact. The deformation structure evolves from impacted, single particles to a coating developed from many impacts. Repeated impacts during cold spray process resulted in a more uniform distribution of deformation in the prior particle interior of the coating compared with that observed in the interior of the single deposited particle (Fig. 12). This result suggests that subsequent impact of powder particles plays a key role in developing the deformation structure in the previously-bonded single particles. In addition, the level of disruption of the θ phase network after cold spray is distinctly different between single, deposited particles and full coatings (Fig. 13). Two Al-5Cu particles are compared in Fig. 13 (a, b) to show the degree of disruption in the θ phase network after impact. The larger particle (about 15 μm in size) impacted onto the substrate with a lower velocity, and consequently presented a relatively intact θ phase network along the cell boundary after deposition. A smaller particle (about 7 μm in size) impacted with a higher velocity and showed an intact network but with some degradation. In the coating, the disruption in the θ phase network at the interface is much more obvious, as the θ phase fragmented into fine θ particles due to the large degree of deformation and repeated impacts by other particles during cold spray. These observations suggest that the degradation and fragmentation of the intermetallic networks in prior powder particles may be caused primarily from repeated impacts by other particles after the initial particle impact.

The ultrafine grains generated by the single particle impact process at the interface between a particle and the substrate or between two prior particles are likely recrystallized grains, as suggested by the low intragranular misorientation in these grains (e.g. see the GROD maps in Figs. 6,7 and 9). An ultrafine grain structure between impacted particles has been reported many times in the cold spray literature [36,44–48]. Many researchers proposed dynamic recrystallization as the formation mechanism of these fine-scale grains, but the exact details for recrystallization during cold spray are still unclear. Rokni et al. [49] has recently reviewed several possible recrystallization mechanisms for cold spray deposition, including continuous dynamic recrystallization (CDRX), geometric dynamic recrystallization (GDRX), rotational dynamic recrystallization (RDRX), static recovery (SRV), and static recrystallization (SRX). CDRX, a purely phenomenological term, referred to recrystallization in ways other than the nucleation and growth of grains, and implied no specific recrystallization mechanism [35]. GDRX and RDRX are two types of CDRX. GDRX described a process of small equiaxed grains formed by serrations and pinching-off of high-angle grain boundaries during deformation. In RDRX, recrystallized grains were created via progressive lattice and subgrain rotation. SRV and SRX are proposed for the formation of ultrafine grains in the cold sprayed bulk deposits, due to the assistance of the residual heat of plastic deformation occurring in subsequent impacts during continued cold spray deposition. In the current paper, we have considered only single particle impacts and still see ultrafine grains at the point of impact without additional impacts. It should also be noted that in Fig. 9, a band of ultrafine grains was observed at the impact between two particles without the impact of a third particle.

The extremely short timescale of the impact process during cold spray (<100 ns) [10] and its effect upon recrystallization must also be considered. Hines et al. [50] proposed a recrystallization mechanism for high strain rate deformation processes based upon rotation recrystallization, termed progressive subgrain misorientation (PriSM) recrystallization. Hines et al. [50,51] investigated recrystallization kinetics within adiabatic shear bands of shock-loaded, pre-strained copper tested at a shear strain rate of 4×10^4 s^{-1}, and argued that the kinetics of classic, diffusion-based recrystallization mechanisms, such as high-angle grain boundary

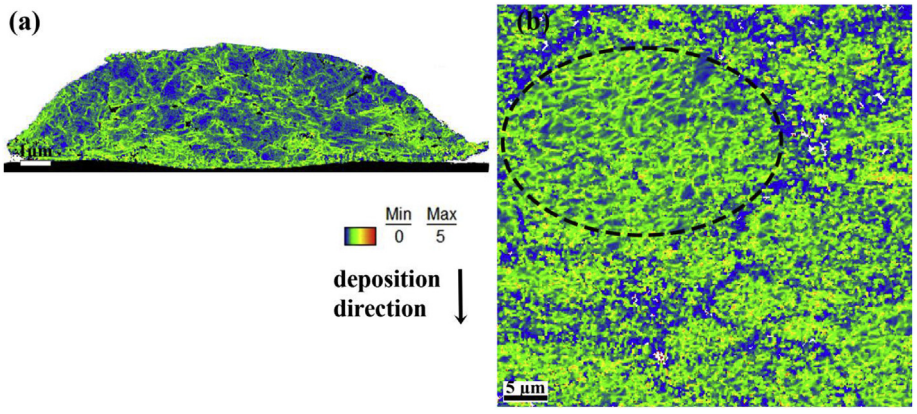

Fig. 12. KAM maps for the Al phase of the Al-5Cu alloy sprayed at 225 °C/1.21 MPa, (a) single deposited particle (PED data), (b) coating (EBSD data), and the black dashed line indicates a prior particle.

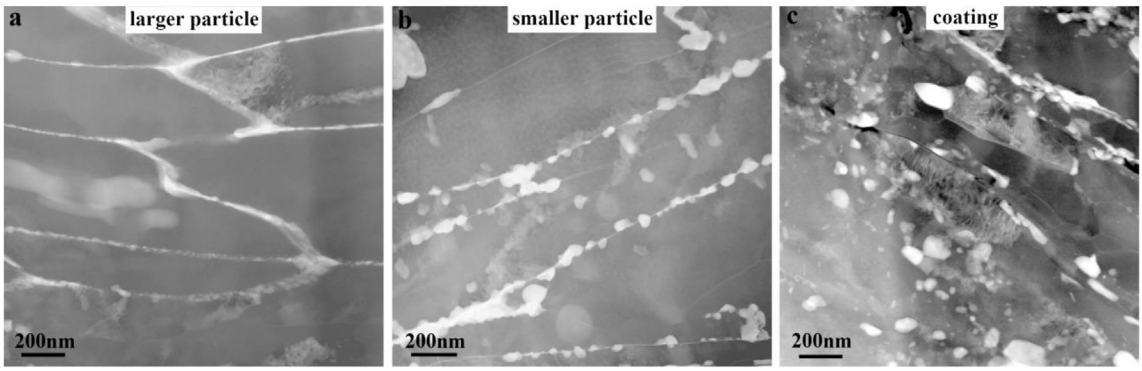

Fig. 13. The morphology of the θ phase network (a, b) near the particle/substrate interface (bottom) of single deposited Al-5Cu particles sprayed at 325 °C/1.21 MPa, (c) in the interfacial region between prior particles of an Al-5Cu coating sprayed at 225 °C/1.21 MPa. It should be noted that the particle width after deformation is approximately 15 μm in (a) and 7 μm in (b), respectively.

migration and subgrain coalescence, were several orders of magnitude slower than the deformation time scale. Further, they suggested PriSM recrystallization was assisted by mechanically driven subgrain rotations with only limited thermal assistance, based on their experiments performed both at room temperature and at liquid nitrogen temperature. As the strain rates involved in the initial cold spray particle impact process (10^6-10^9 s^{-1}) are much higher than the work of Hines et al., it is even more important to consider recrystallization mechanisms that do not require thermal diffusion. This is not to say that thermal diffusion-based recrystallization is not operative during subsequent impacts or simply by heating of the deposit microstructure during the rest of the cold spray process. However, as individual particle impacts occur at extremely high strain rates and short times, a diffusionless recrystallization mechanism seems highly likely, and further research will be important to develop a more detailed recrystallization model for the cold spray process.

The cold spray literature and the results of the current paper suggest that the nature of the interface between an impacted particle and the substrate [6–9,52] may be material-system dependent. The Al-Cu particles and the steel substrate were bonded via a thin amorphous layer at the interface (Fig. 10). Likewise, Ko et al. [52] revealed a firmly attached coating when spraying aluminum particles onto steel, and observed that a thin and amorphous Al-Fe intermixed layer was generated along the interface. We have also observed in the current study that the interface between two Al-2Cu particles was intimately bonded with no amorphous layer in between. Kang et al. [9] studied cold spraying of individual aluminum particles onto Al 1050 alloy substrates, and observed a strong metallic bonding at the particle/substrate interface, without an amorphous layer. In the titanium system, Kim et al. [8] studied bonding mechanisms in modified cold spraying using preheated titanium powder particles onto different substrates. They found that titanium substrates and titanium particles formed direct metallurgical bonding without any interfacial layer or oxide, however, on an aluminum substrate, the titanium particles were not heavily deformed, the oxide on the titanium particle surface was retained, and there was an amorphous layer with embedded nano grains in the interfacial region between the titanium particles and the aluminum substrate.

5. Conclusion

The impact deformation behavior of single, cold sprayed Al-Cu particles and the interface microstructure between the sprayed particle and the substrate have been examined, and the conclusions are summarized as follows:

1. The Al-Cu particles are heavily deformed upon impact, and the average compression ratio is approximately 0.52–0.59.
2. The compression ratio did not show a significant dependence on increasing copper content. The average compression ratio of Al-2Cu alloy with a value of 0.59 was only slightly higher than that of Al-5Cu alloy with a value of 0.55.
3. The deformation was not evenly distributed across the entire particle, but increased significantly towards the particle/substrate interface.
4. Ultrafine grains (<500 nm diameter) were formed at the interfacial region between particle and substrate, likely via dynamic recrystallization during the single particle impact process. A similar band of ultrafine grains was observed at the interface between two Al-2Cu particles that impacted.
5. A thin (10–15 nm) amorphous layer was observed at the interface between single Al-Cu particles and the steel substrate, while the interface between impacted aluminum particles did not show an amorphous layer.

Acknowledgements

This research was supported by funding from Mr. William Nickerson of the Office of Naval Research (Code 35 Sea-Based Aviation Structures and Materials, N0001414WX00148) and the funding from the college of engineering at the University of Alabama. We thank N.C. Machado Da Rocha for her assistance in focused ion beam milling and scanning electron microscopy imaging. We thank Prof. J.C. Hooper, Dr. S. Menon and R. Chisholm for their assistance with the pure aluminum and copper particle impact samples.

References

[1] A. Alkimov, Gas Dynamic Spraying Method for Applying a Coating, 1994. US Pat. No. 5302414.
[2] P.C. King, G. Bae, S.H. Zahiri, M. Jahedi, C. Lee, An experimental and finite element study of cold spray copper impact onto two aluminum substrates, J. Therm. Spray Technol. 19 (3) (2010) 620–634.
[3] T. Schmidt, F. Gärtner, H. Assadi, H. Kreye, Development of a generalized parameter window for cold spray deposition, Acta Mater. 54 (3) (2006) 729.
[4] H. Assadi, T. Schmidt, H. Richter, J.O. Kliemann, K. Binder, F. Gärtner, T. Klassen, H. Kreye, On parameter selection in cold spraying, J. Therm. Spray Technol. 20 (6) (2011) 1161.
[5] M. Hassani-Gangaraj, D. Veysset, K.A. Nelson, C.A. Schuh, In-situ observations of single micro-particle impact bonding, Scripta Mater. 145 (2018) 9–13.
[6] H. Assadi, F. Gärtner, T. Stoltenhoff, H. Kreye, Bonding mechanism in cold gas spraying, Acta Mater. 51 (15) (2003) 4379–4394.
[7] Y. Xiong, K. Kang, G. Bae, S. Yoon, C. Lee, Dynamic amorphization and

recrystallization of metals in kinetic spray process, Appl. Phys. Lett. 92 (19) (2008) 194101.
[8] K. Kim, M. Watanabe, S. Kuroda, Bonding mechanisms of thermally softened metallic powder particles and substrates impacted at high velocity, Surf. Coating. Technol. 204 (14) (2010) 2175–2180.
[9] K. Kang, J. Won, G. Bae, S. Ha, C. Lee, Interfacial bonding and microstructural evolution of Al in kinetic spraying, J. Mater. Sci. 47 (11) (2012) 4649–4659.
[10] P.C. King, G. Bae, S.H. Zahiri, M. Jahedi, C. Lee, An experimental and finite element study of cold spray copper impact onto two aluminum substrates, J. Therm. Spray Technol. 19 (3) (2009) 620.
[11] G. Bae, J.-i. Jang, C. Lee, Correlation of particle impact conditions with bonding, nanocrystal formation and mechanical properties in kinetic sprayed nickel, Acta Mater. 60 (8) (2012) 3524–3535.
[12] X. Suo, M. Yu, W. Li, M. Planche, H. Liao, Effect of substrate preheating on bonding strength of cold-sprayed Mg coatings, J. Therm. Spray Technol. 21 (5) (2012) 1091–1098.
[13] P.C. King, C. Busch, T. Kittel-Sherri, M. Jahedi, S. Gulizia, Interface melding in cold spray titanium particle impact, Surf. Coating. Technol. 239 (2014) 191.
[14] M.V. Vidaller, A. List, F. Gaertner, T. Klassen, S. Dosta, J.M. Guilemany, Single impact bonding of cold sprayed Ti-6Al-4V powders on different substrates, J. Therm. Spray Technol. 24 (4) (2015) 644–658.
[15] X. Song, J. Everaerts, W. Zhai, H. Zheng, A.W.Y. Tan, W. Sun, F. Li, I. Marinescu, E. Liu, A.M. Korsunsky, Residual stresses in single particle splat of metal cold spray process–Numerical simulation and direct measurement, Mater. Lett. 230 (2018) 152–156.
[16] M. Hassani-Gangaraj, D. Veysset, V.K. Champagne, K.A. Nelson, C.A. Schuh, Adiabatic shear instability is not necessary for adhesion in cold spray, Acta Mater. 158 (2018) 430–439 .
[17] H. Assadi, F. Gärtner, T. Klassen, H. Kreye, Comment on 'Adiabatic shear instability is not necessary for adhesion in cold spray', Scripta Mater. 162 (2018) 512–514 .
[18] M. Hassani-Gangaraj, D. Veysset, V.K. Champagne, K.A. Nelson, C.A. Schuh, Response to Comment on "Adiabatic shear instability is not necessary for adhesion in cold spray", Scripta Mater. 162 (2018) 515–519.
[19] W.-Y. Li, H. Liao, C.-J. Li, G. Li, C. Coddet, X. Wang, On high velocity impact of micro-sized metallic particles in cold spraying, Appl. Surf. Sci. 253 (5) (2006) 2852–2862.
[20] W.-Y. Li, H. Liao, C.-J. Li, H.-S. Bang, C. Coddet, Numerical simulation of deformation behavior of Al particles impacting on Al substrate and effect of surface oxide films on interfacial bonding in cold spraying, Appl. Surf. Sci. 253 (11) (2007) 5084–5091.
[21] P.C. King, S.H. Zahiri, M. Jahedi, Microstructural refinement within a cold-sprayed copper particle, Metall. Mater. Trans. 40 (9) (2009) 2115.
[22] P.C. King, M. Jahedi, Relationship between particle size and deformation in the cold spray process, Appl. Surf. Sci. 256 (6) (2010) 1735–1738.
[23] A. Alkhimov, S. Klinkov, V. Kosarev, Experimental study of deformation and attachment of microparticles to an obstacle upon high-rate impact, J. Appl. Mech. Tech. Phys. 41 (2) (2000) 245–250.
[24] R.R. Keller, R.H. Geiss, Transmission EBSD from 10 nm domains in a scanning electron microscope, J. Microsc. 245 (3) (2012) 245–251.
[25] G.C. Sneddon, P.W. Trimby, J.M. Cairney, Transmission Kikuchi diffraction in a scanning electron microscope: a review, Mater. Sci. Eng. R Rep. 110 (2016) 1–12.
[26] R. Vincent, P. Midgley, Double conical beam-rocking system for measurement of integrated electron diffraction intensities, Ultramicroscopy 53 (3) (1994) 271–282.
[27] A. Garner, A. Gholinia, P. Frankel, M. Gass, I. MacLaren, M. Preuss, The microstructure and microtexture of zirconium oxide films studied by transmission electron backscatter diffraction and automated crystal orientation mapping with transmission electron microscopy, Acta Mater. 80 (2014) 159–171.
[28] T. Liu, J.D. Leazer, S.K. Menon, L.N. Brewer, Microstructural Analysis of Gas Atomized Al-Cu Alloy Feedstock Powders for Cold Spray Deposition, Surface and Coatings Technology, 2018.
[29] D. Viladot, M. Véron, M. Gemmi, F. Peiró, J. Portillo, S. Estradé, J. Mendoza, N. Llorca-Isern, S. Nicolopoulos, Orientation and phase mapping in the transmission electron microscope using precession-assisted diffraction spot recognition: state-of-the-art results, J. Microsc. 252 (1) (2013) 23–34.
[30] S.I. Wright, M.M. Nowell, D.P. Field, A review of strain analysis using electron backscatter diffraction, Microsc. Microanal. 17 (3) (2011) 316–329.
[31] L. Brewer, M. Othon, L. Young, T. Angeliu, Misorientation mapping for visualization of plastic strain via electron back-scattered diffraction, Microsc. Microanal. 8 (S02) (2002) 684–685.
[32] L. Brewer, M. Othon, L. Young, T. Angeliu, Misorientation mapping for visualization of plastic deformation via electron back-scattered diffraction, Microsc. Microanal. 12 (1) (2006) 85–91.
[33] M. Drury, F. Humphreys, The development of microstructure in Al-5% Mg during high temperature deformation, Acta Metall. 34 (11) (1986) 2259–2271.
[34] M. Meyers, Y. Xu, Q. Xue, M. Perez-Prado, T. McNelley, Microstructural evolution in adiabatic shear localization in stainless steel, Acta Mater. 51 (5) (2003) 1307–1325.
[35] F.J. Humphreys, M. Hatherly, Recrystallization and Related Annealing Phenomena, Elsevier, 2004.
[36] Y. Zou, W. Qin, E. Irissou, J.-G. Legoux, S. Yue, J.A. Szpunar, Dynamic recrystallization in the particle/particle interfacial region of cold-sprayed nickel coating: electron backscatter diffraction characterization, Scripta Mater. 61 (9) (2009) 899–902.
[37] W. Wong, P. Vo, E. Irissou, A. Ryabinin, J.-G. Legoux, S. Yue, Effect of particle morphology and size distribution on cold-sprayed pure titanium coatings, J. Therm. Spray Technol. 22 (7) (2013) 1140–1153.
[38] D. Gilmore, R. Dykhuizen, R. Neiser, M. Smith, T. Roemer, Particle velocity and deposition efficiency in the cold spray process, J. Therm. Spray Technol. 8 (4) (1999) 576–582.
[39] J.D. Leazer, Processing-microstructure-property Relationships for Cold Spray Powder Deposition of Al-Cu Alloys, NAVAL POSTGRADUATE SCHOOL MONTEREY CA, 2015.
[40] R. Huang, H. Fukanuma, Study of the influence of particle velocity on adhesive strength of cold spray deposits, J. Therm. Spray Technol. 21 (3–4) (2012) 541–549.
[41] D. Poirier, J.-G. Legoux, R.A. Drew, R. Gauvin, Consolidation of Al 2 O 3/Al nanocomposite powder by cold spray, J. Therm. Spray Technol. 20 (1–2) (2011) 275–284.
[42] Y. Zou, D. Goldbaum, J.A. Szpunar, S. Yue, Microstructure and nanohardness of cold-sprayed coatings: electron backscattered diffraction and nanoindentation studies, Scripta Mater. 62 (6) (2010) 395–398.
[43] F. Yang, A. Saxena, L. Riester, Use of the nanoindentation technique for studying microstructure/crack interactions in the fatigue of 4340 steel, Metall. Mater. Trans. 29 (12) (1998) 3029–3036.
[44] M. Rokni, C. Widener, G. Crawford, Microstructural evolution of 7075 Al gas atomized powder and high-pressure cold sprayed deposition, Surf. Coating. Technol. 251 (2014) 254–263.
[45] M. Rokni, C. Widener, V. Champagne, Microstructural evolution of 6061 aluminum gas-atomized powder and high-pressure cold-sprayed deposition, J. Therm. Spray Technol. 23 (3) (2014) 514–524.
[46] A.C. Hall, L.N. Brewer, Preparation of Aluminum Coatings Containing Homogenous Nanocrystalline Microstructures Using the Cold Spray Process..
[47] K. Kim, M. Watanabe, J. Kawakita, S. Kuroda, Grain refinement in a single titanium powder particle impacted at high velocity, Scripta Mater. 59 (7) (2008) 768–771.
[48] G. Bae, K. Kang, J.-J. Kim, C. Lee, Nanostructure formation and its effects on the mechanical properties of kinetic sprayed titanium coating, Mater. Sci. Eng. 527 (23) (2010) 6313.
[49] M. Rokni, S. Nutt, C. Widener, V. Champagne, R. Hrabe, Review of relationship between particle deformation, coating microstructure, and properties in high-pressure cold spray, J. Therm. Spray Technol. 26 (6) (2017) 1308–1355.
[50] J.A. Hines, K.S. Vecchio, S. Ahzi, A model for microstructure evolution in adiabatic shear bands, Metall. Mater. Trans. 29 (1) (1998) 191–203.
[51] J. Hines, K. Vecchio, Recrystallization kinetics within adiabatic shear bands, Acta Mater. 45 (2) (1997) 635–649.
[52] K.H. Ko, J.O. Choi, H. Lee, Intermixing and interfacial morphology of cold-sprayed Al coatings on steel, Mater. Lett. 136 (2014) 45.